Macromolecular Rapid Communications
www.mrc-journal.de

Tailoring Microstructure and Morphology via Sequential Fluorination to Enhance the Photovoltaic Performance of Low-Cost Polymer Donors for Organic Solar Cells

*Gururaj P. Kini, Yong Woon Han, Sung Jae Jeon, Eui Jin Lee, Yoon Jae Lee, Munju Goh, and Doo Kyung Moon**

For utilizing organic solar cells (OSCs) for commercial applications, reducing the overall cost of the photo absorbent materials is also very crucial. Herein, such a challenge is addressed by synergistically controlling the amount of fluorine (F)-substituents ($n = 2, 4$) on a low-cost wide-bandgap molecular design involving alternate fluorinated-thienyl benzodithiophene donor and 2,5-difluoro benzene (2FBn) or 2,3,5,6 tetrafluorobenzene (4FBn) to form two new polymer donors PBDT-2FBn and PBDT-4FBn, respectively. As expected, sequential fluorination causes a lowering of the frontier energy levels and planarization of polymer backbone via F···S and C-H···F noncovalent molecular locks, which results in more pronounced molecular packing and enhanced crystallinity from PBDT-2FBn to PBDT-4FBn. By mixing with IT-4F acceptor, PBDT-2FBn:IT-4F-based blend demonstrates favorable molecular orientation with shorter π–π stacking distance, higher carrier mobilities and desirable nanoscale morphology, hence delivering a higher power conversion efficiency (PCE) of 9.3% than PBDT-2FBn:IT-4F counterpart (8.6%). Furthermore, pairing PBDT-2FBn with BTP-BO-4Cl acceptor further improved absorption range and promoted privileged morphology for efficient exciton dissociation and charge transport, resulting in further improvement of PCE to 10.2% with remarkably low energy loss of 0.46 eV. Consequently, this study provides valuable guidelines for designing efficient and low-cost polymer donors for OSC applications.

1. Introduction

Recently, organic solar cells (OSCs) comprising of bulk heterojunction layer of electron donor and electron acceptor have been evolved to be emerging renewable energy resources because of their excellent application prospects, including lightweight, low-cost large-area roll-to-roll solution processing on a flexible substrate and employing them in both indoor and semi-transparent application.[1–7] During the last 3 years, rapid growth in the molecular strategies to construct state-of-the-art low bandgap (LBG) non-fullerene small molecular acceptors (NFA) has been realized,[8–14] which plays a pivotal role in boosting OSC's power conversion efficiencies (PCEs) up to 17%.[5,15–18] Hence, the development of novel polymer donors well-matching with emerging NFAs is crucial for realizing efficient and practical OSCs. Currently, the progress of polymer donors for OSCs is essentially dependent on two significant factors. First, most of these reported efficient NFAs exhibit the lowest unoccupied molecular orbital (LUMO), which negatively affects their lower open-circuit voltage (V_{oc}) in corresponding OSCs devices.[19–21] Hence, feasible molecular strategies to effectively lower the highest occupied molecular orbital (HOMO) energy levels without varying bandgap are essential, which can realize higher V_{oc}.[22,23] Second, the synthesis of high-performing polymer donors such as PM6, D18, PTzBI-*d*F, or PBQ6 would unavoidably use expensive fused monomers having multistep synthesis and purification processes with lower yields, resulting in poor scalability at low cost for large-scale production (Figure S4, Supporting Information).[24,25] Thus, the development of the novel wide bandgap (WBG) donors possessing deeper HOMO levels and complementary absorption profiles with these NFAs, and having a simple molecular design is recognized as the most practical way to boost the efficiency and reduce the overall cost, simultaneously.

Based on a similar approach, our group previously showed that 2,5-difluoro benzene (2FBn) could serve as a low-cost building block used to synthesize BDT-alt-heteroarene-type WBG donor polymer.[26] We demonstrated that aromatic benzene having fluorine (F)-substituents not only deep frontier molecular energy levels with high optical bandgap (E_g^{opt}), but also noncovalent fluorine (F)···sulfur (S) and carbon (C)-hydrogen (H)···F noncovalent

G. P. Kini, Y. W. Han, S. J. Jeon, E. J. Lee, Y. J. Lee, D. K. Moon
Nano and Information Materials (NIMs) Laboratory
Department of Chemical Engineering
Konkuk University
120, Neungdong-ro, Gwangjin-gu, Seoul 05029, Korea
E-mail: dkmoon@konkuk.ac.kr
M. Goh
Department of Chemical Engineering
Konkuk University
120, Neungdong-ro, Gwangjin-gu, Seoul 05029, Korea
The ORCID identification number(s) for the author(s) of this article can be found under https://doi.org/10.1002/marc.202200070

DOI: 10.1002/marc.202200070

inter/intramolecular confirmation locks further ensured coplanar backbone, higher crystallinity, and charge carrier mobility. Besides, the synthesis of 2FBn acceptor units involves facile three-step synthesis. Hence, the corresponding polymer PBDT-2FBnT produced an excellent PCE of 9.5% with a compatible 3,9-bis(2-methylene-(3-(1,1-dicyanomethylene)-indanone))-5,5,11,11-tetrakis(4-hexylphenyl)-dithieno[2,3-d:2',3'-d']-s-indaceno[1,2-b:5,6-b']dithiophene (ITIC) acceptor. Notably, due to the use of unsubstituted 2D benzo[1,2-b:4,5-b′]dithiophene (2D-BDT) unit (which has intrinsic electron donating characteristics enabled by the 2D-thienyl units), PBDT-2FBnT showed relatively higher HOMO energy levels than emerging 3,9-bis(2-methylene-((3-(1,1-dicyanomethylene)-6,7-difluoro)-indanone))-5,5,11,11-tetrakis(4-hexylphenyl)-dithieno[2,3-d:2',3'-d']-s-indaceno[1,2-b:5,6-b']dithiophene (IT-4F) or Y-type NFAs, suggesting there is further room for improving the PCEs if we could optimize the molecular structure of PBDT-2FBnT by maintaining E_g^{opt} and further lowering the HOMO to match IT-4F or Y-type NFAs. Recently, introducing various functional groups such as F,[19,21,25,27–31] chlorine,[6,29] sulfur,[32–36] and silicon,[37–39] on 2D-thienyl side-chains of BDT is a proven strategy for further lowering HOMO energy levels of BDT-based polymer donors. Among these, introducing F-substituents has advantages such as reducing energy levels, enhancing absorption coefficient, molecular planarity, and crystallinity.[5,26,40–48] Therefore, fluorinated-thienyl BDT donor units (2FBDT) were exclusively utilized for designing highly efficient WBG polymers donors.[19,21,25,27–30] Likewise, insertion of low-cost fluorinated benzene units having different amounts of F-substituents in molecular design will also offer good tailoring of photophysical properties and aggregation behavior along with much more straightforward synthesis. Various recent works demonstrate the effectiveness of this strategy for the development of polymer donors.[42,46,49–52] Thus, considering the above-discussed facts, we attempted to optimize the rational molecular design of PBDT-2FBnT by synergistically introducing F-BDT and 2FBn or 1,4-dibromo-2,3,5,6 tetrafluorobenzene (4FBn) units for the construction of efficient, low-cost non-fullerene OSCs, as shown in **Figure 1**a.

In this work, we report two new low-cost WBG polymer donors, namely poly-{4,8-bis(5-(2-ethylhexyl)-4-fluorothiophen-2-yl)-2-(3-(2-ethylhexyl)-5-(4-(4-(2-ethylhexyl)-5-methylthiophen-2-yl)-2,5-difluorophenyl)thiophen-2-yl)-6-methylbenzo[1,2-b:4,5-b′]dithiophene (PBDT-2FBn) and poly-{4,8-bis(5-(2-ethylhexyl)-4-fluorothiophen-2-yl)-2-(3-(2-ethylhexyl)-5-(4-(4-(2-ethylhexyl)-5-methylthiophen-2-yl)-2,3,5,6-tetrafluorophenyl)thiophen-2-yl)-6-methylbenzo[1,2-b:4,5-b′]dithiophene) (PBDT-4FBn) having alternate F-BDT as "D" and alkyl-substituted 2FBn or 4FBn as "A" units, respectively. These polymers have a simple three-step synthesis starting from commercially available inexpensive 2FBn or 4FBn units, thereby reducing overall synthetic cost (Figure S4, Supporting Information). As expected, enabled by varying the number of F-substituents, PBDT-2FBn and PBDT-4FBn displayed a deep-lying HOMO level of −5.52 and −5.63 eV, respectively, resulting in a good match with emerging IT-4F or BTP-BO-4Cl acceptor units. Moreover, systematic investigations revealed that sequential fluorination from PBDT-2FBn and PBDT-4FBn enhanced molecular planarity and crystallinity by F···S and C-H···F confirmation locks, which agrees well with our hypothesis. By blending with IT-4F acceptor, optimal PBDT-2FBn:IT-4F-based devices delivered a higher PCE of 9.3% than PBDT-4FBn:IT-4F-based devices (8.6%). Moreover, by mixing PBDT-4FBn with BTP-BO-4Cl, the efficiency was further enhanced to 10.2%. Different energy level alignment of these two molecules and their distinctive behavior at solid-state were the major reasons behind their different photovoltaic performance, supported by diverse characterization techniques as discussed below.

2. Result and Discussion

The synthesis of monomers, 5,5′-(2,5-difluoro-1,4-phenylene)bis(2-bromo-3-(2-ethylhexyl)thiophene) (M1), 5,5′-(perfluoro-1,4-phenylene)bis(2-bromo-3-(2-ethylhexyl)thiophene) (M2), and polymers is shown in Figure 1b,c, and their detailed synthetic procedures including characterization are given in Supporting Information. First, tributyl(4-(2-ethylhexyl)thiophen-2-yl)stannane (3) was coupled with commercially available low-cost starting materials 1,4-dibromo-2,5-difluorobenzene (1) and 1,4-dibromo-4FBn (2) to obtain intermediate 4 and 5, and both products were subsequently brominated using *N*-bromosuccinimide to produce final monomers M1 and M2, respectively (two-step yield >80%). Then, copolymerization of M1 or M2 with (4,8-bis(5-(2-ethylhexyl)-4-fluorothiophen-2-yl)benzo[1,2-b:4,5-b']dithiophene-2,6-diyl)bis(trimethylstannane) (FBDT-Sn) via Stille polycondensation reaction delivered the polymers PBDT-2FBn and PBDT-4FBn, respectively, with yields over 80%. The molecular weights of the polymers were determined using gel permeation chromatography (GPC) against polystyrene standards. The number-average molecular weights (M_n)/polydispersity indices of PBDT-2FBn and PBDT-4FBn were 29.2kDa/2.24 and 22.5kDa/1.95, respectively. As good thermal stability of polymers is of great importance for utilizing polymers in OSCs application, the thermogravimetric analysis of two polymers was studied (Figure S5, Supporting Information). PBDT-2FBn and PBDT-4FBn displayed good thermal stability with a decomposition temperature (Td, 5% weight loss under nitrogen atmosphere) of 434 and 397 °C, respectively.

As shown in **Figure 2**, optimized geometries and electronic structures of methyl-substituted dimers structures of PBDT-2FBn and PBDT-4FBn were predicted using density functional theory (DFT) calculations at the B3LYP/6-31g(d) level. Notably, both polymers showed relatively similar torsion angles (θ_1 and $\theta_4 \approx 22$–$27°$) between FBDT and adjacent thiophene units. In contrast, the dihedral angle between 2Fbn or 4FBn and adjacent thiophene display marked differences. The 4FBn-based PBDT-4FBn has a much smaller dihedral angle (θ_2 and $\theta_3 = 1.11°$ and 6.48°, respectively) than 2FBn-based PBDT-2FBn (θ_2 and $\theta_3 = 13.92$ and 14.89°, respectively). These results were ascribed from the F-induced noncovalent S···F and S···H conformational locks, which significantly improve the coplanarity of the polymer backbone, as reported in previous reports.[26,42,46,51] Thus, PBDT-4FBn has enhanced coplanarity than PBDT-2FBn as depicted in the side-view, which is expected to have marked effects on molecular packing and bulk morphologies. Meanwhile, frontier molecular orbitals energy levels profile of both polymers

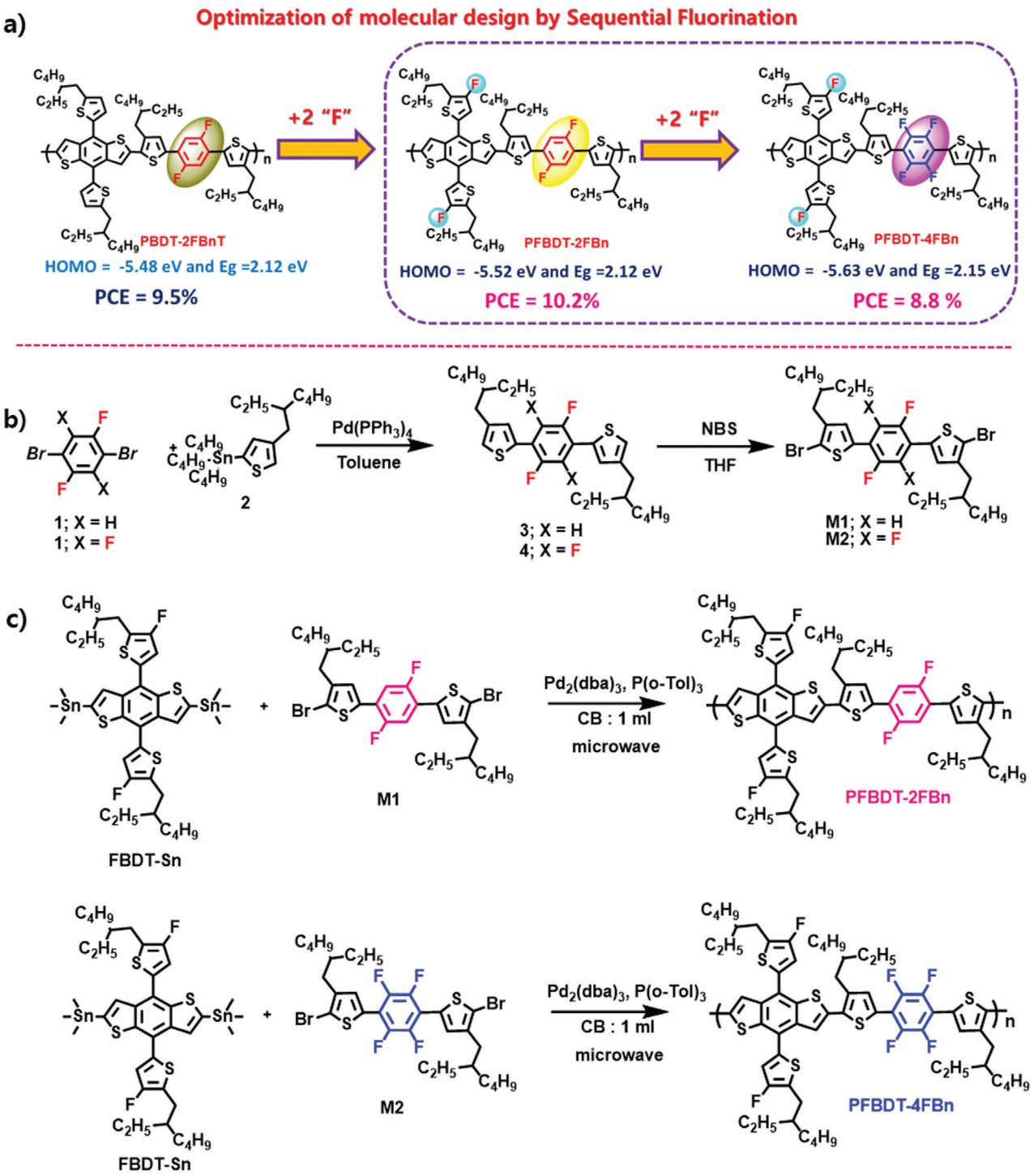

Figure 1. a) Chemical structures of the new polymers reported in this work. Synthetic routes of b) monomers and c) polymers PBDT-2FBn and PBDT-4FBn.

displayed similar electron density distribution along the backbone, where HOMO and LUMO are delocalized over the entire conjugated backbone. Besides, owing to a higher degree of electronegative F-atoms; calculated HOMO/LUMO energy levels of PBDT-4FBn were found to be −5.05/−2.44 eV, which were lower than PBDT-2FBn counterparts (−4.98/−2.35 eV) and consistent with the cyclic voltammetry measurements (discussed below). Thus, deep HOMO energy levels of PBDT-4FBn are expected to enhance V_{oc} in the corresponding OSCs.

Figures 3a and b show the ultraviolet–visible (UV–vis) absorption spectra of PBDT-2FBn and PBDT-4FBn in chloroform solutions and thin-film states, respectively, while corresponding

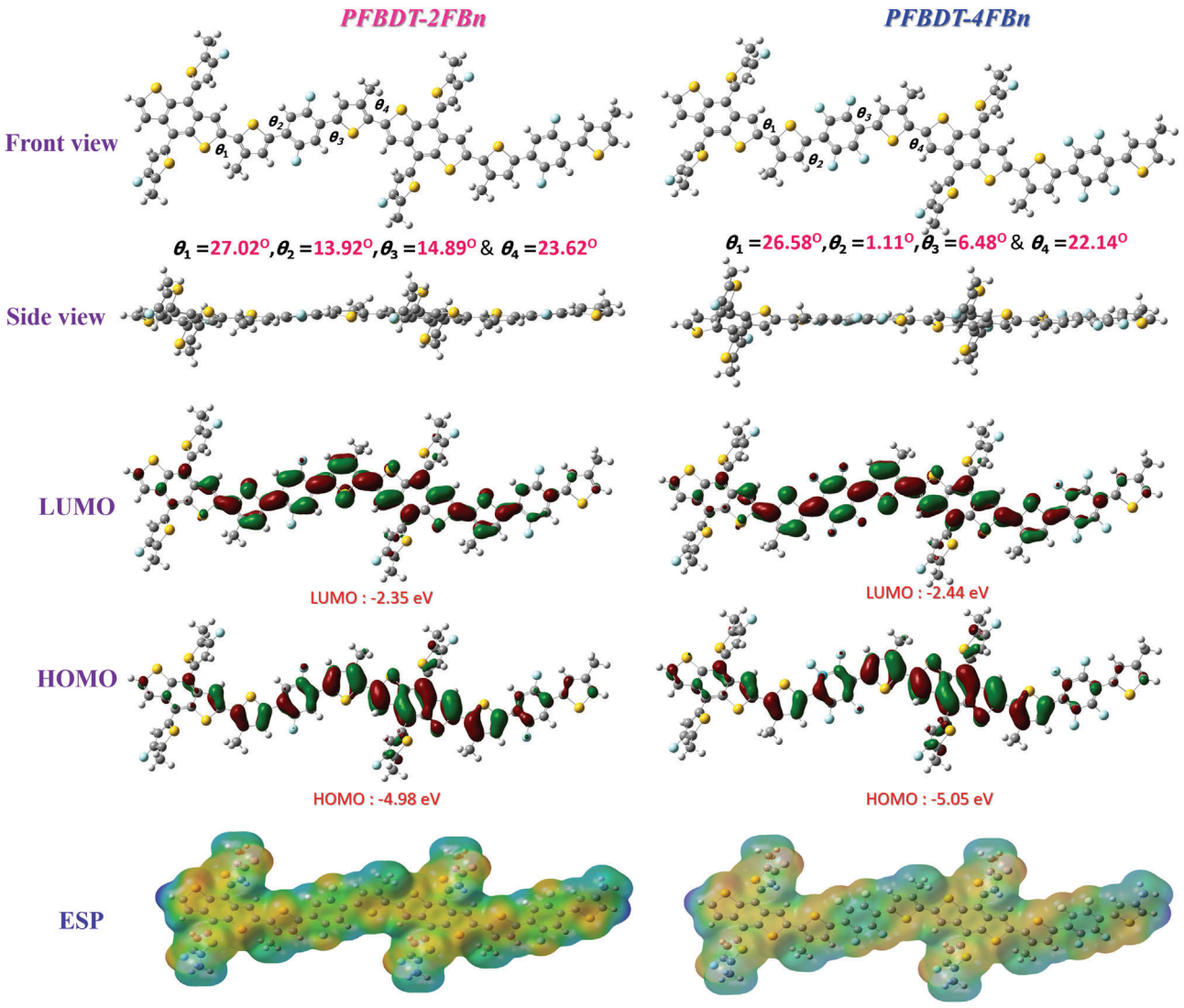

Figure 2. DFT optimized molecular geometries, frontier energy levels, and ESP profiles of the methyl-substituted dimers of the PBDT-2FBn and PBDT-4FBn polymers.

photophysical parameters are tabulated in **Table 1**. In the solution state, these polymers exhibit similar absorption profiles ranging from 300 to 550 nm with maximum absorption peaks at 495 and 505 nm for PBDT-2FBn and PBDT-4FBn, respectively. The molar absorption coefficients (ϵ) of the polymers were calculated to be 6.62×10^4 M^{-1} cm^{-1} (495 nm) and 5.79×10^4 M^{-1} cm^{-1} (505 nm) for PBDT-2FBn and PBDT-4FBn, respectively, from the UV–vis data on chloroform solutions with different concentrations on the order of 10^{-5} M and the Beer–Lambert equation (Figure S6, Supporting Information). In the film state, the absorption profile of polymers becomes much broader, and they display prominent vibronic peaks, indicating stronger intermolecular π–π stacking. However, there was no significant shift in the absorption maxima from the solution to film state, suggesting molecular packing arrangements of aggregates are not incredibly varied by solidification.[53] Meanwhile, for PBDT-2FBn, the film showed a more substantial absorption aggregation peak at 541 nm and a weaker peak at 504 nm, revealing it has a stronger J-aggregation (originates from end-to-end molecular arrangements).[54,55] In contrast. PBDT-4FBn displayed opposite trends, that is, the peak ascribed from H-aggregation (ascribed from face-to-face molecular arrangements) at 502 nm was more potent than that of the *J*-aggregation peak at 538 nm.[54] The E_g^{opt} calculated from absorption onsets at 585 nm of PBDT-2FBn and 577 nm of PBDT-4FBn in film state were 2.12 and 2.15 eV, respectively.

The cyclic voltammetry method was employed to estimate the electrochemical properties of the polymers against ferrocene as internal standards. From the cyclic voltammograms Figure 3c, HOMO and LUMO were calculated from polymers onsets oxidation and reduction potential, respectively. The calculated HOMO and LUMO energy levels are −5.52/−3.50 and −5.63/−3.57 eV for PBDT-2FBn and PBDT-4FBn, respectively. As expected, originating from the insertion of higher F-substituents with high electronegativity, PBDT-4FBn demonstrated both deeper HOMO and LUMO energy levels than PBDT-2FBn. Meanwhile, both polymers showed complementary absorption and cascade energy

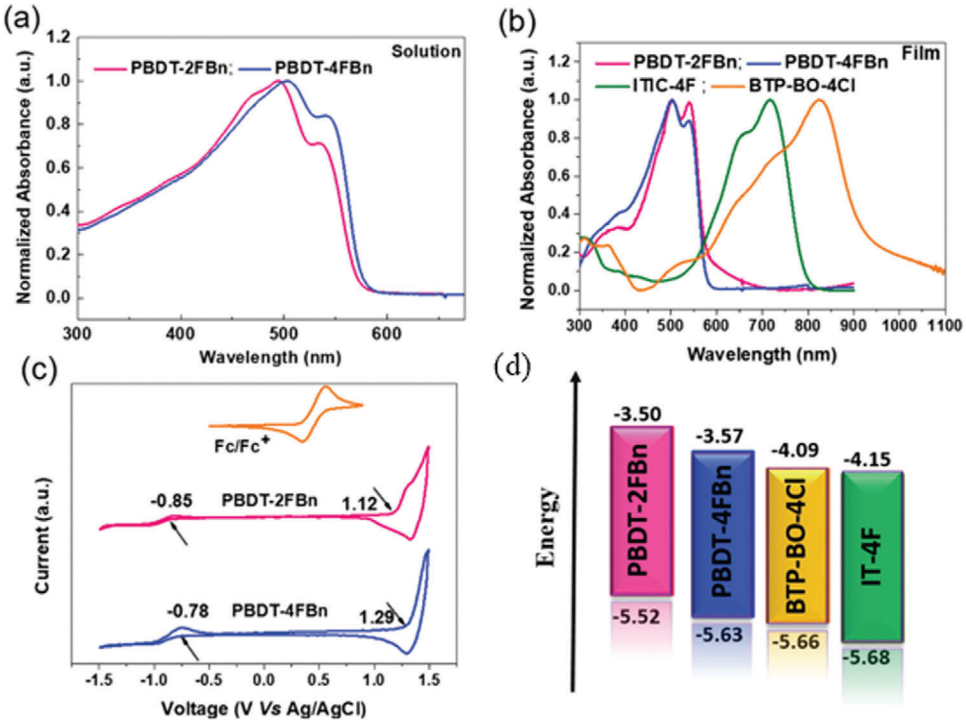

Figure 3. Normalized absorption profiles of the polymers in a) chloroform solution, b) the thin-film state, c) corresponding cyclic voltammograms, and d) energy level alignment of polymers and non-fullerene acceptors used in this study.

Table 1. The optical properties and frontier energy levels of PBDT-2FBn and PBDT-4FBn.

Polymer	M_n [kDa]/PDI[a)]	Optical properties					Electrochemical properties	
		λ_{max} [nm], solution	ϵ [10^4] [M^{-1} cm^{-1}][b)]	λ_{max} [nm], thin film	λ_{onset} [nm], thin film	E_g^{opt} [eV][c)]	HOMO [eV][CV]	LUMO [eV][CV]
PBDT-2FBn	29.2/2.24	495, 535	6.62 (at 495 nm)	504, 541	585	2.12	−5.52	−3.50
PBDT-4FBn	22.5/1.95	505, 545	5.79 (at 505 nm)	502, 538	577	2.15	−5.63	−3.57

[a)] Measured by GPC. [b)] The molar extinction coefficient of the polymers in CF solution was measured using the Beer–Lambert law ($A = \epsilon bc$). [c)] $E_g^{opt} = 1240/\lambda_{onset}$ (neat film), eV.

level alignment with popular non-fullerene acceptors IT-4F and BTP-BO-4Cl (Figure 3b,d). Thus, mixing these blend components is predicted to yield efficient exciton dissociation and effective solar energy harvesting by covering a broad absorption range.

The photovoltaic properties of both polymers were tested by mixing with IT-4F acceptor units. Initially, device structure, blend ratio, and spin coating speed were fully optimized to realize the best composition. Both optimized inverted (ITO/ZnO/active layer/MoO_3/Ag) and conventional (ITO/PEDOT:PSS/active layer/PDINN/Ag) devices were fabricated using donor/acceptor weight ratio of 1:1, and CB with 0.5 vol% DIO as a solvent additive, however, the postannealing temperature was 140 °C for 10 min for inverted and 100 °C for 10 min for conventional devices (Figures S6 and S7 and Tables S1 and S2, Supporting Information). The current density–voltage (J–V) curves of the optimized devices under AM 1.5G illumination are shown in **Figure 4**, with the corresponding data summarized in **Table 2**. The inverted devices with PBDT-2FBn:IT-4F produced the best PCE of 9.1% with V_{oc} of 0.838 V, short-circuit current density (J_{SC}) of 18.3 mA cm^{-2}, and fill factor (FF) of 59.3%, while PBDT-4FBn:IT-4F-based devices showed slightly higher V_{oc} of 0.899 V but decreased J_{sc} of 17.3 mA cm^{-2} and FF of 55.1%, realizing PCE of 8.6%. Likewise, in the conventional conditions, PBDT-2FBn and PBDT-4FBn produced maximum PCE of 9.3% and 8.2%, with slight variation in photovoltaic parameters shown in Table 2. Based on these results, it is evident that though device configuration has marginal effects on improving the overall performance in both blends, interestingly, they have distinct trends in both cases. In the case of PBDT-2FBn:IT-4F-based blend films, higher PCEs of conventional devices are attributed to the slightly higher V_{oc} and FF compared to the inverted counterpart. However, these trends were reversed in the case of PBDT-4FBn:IT-4F films, where improved performances were seen in an inverted configuration. Notably, these enhancements

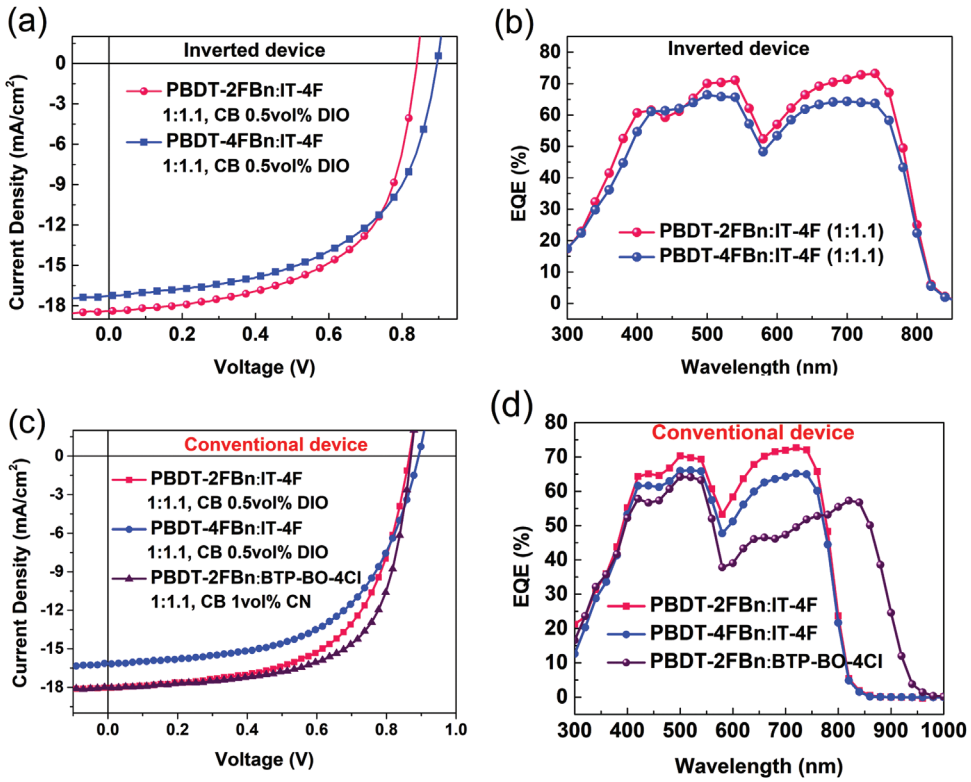

Figure 4. a,c) The *J–V* curves and b,d) of optimal OSCs based on PBDT-2FBn:IT-4F, PBDT-4FBn:IT-4F, and PBDT-2FBn:BTP-BO-4Cl-based blends fabricated with different device architecture.

Table 2. The photovoltaic parameters of the optimized devices under AM 1.5G illumination at (100 mW cm^{-2}) were processed using inverted and conventional device configuration.

Blend	Device structure	Solvent	V_{oc} [V]	J_{SC} [mA cm^{-2}] [Cal. J_{SC}][a)]	FF [%]	PCE[a] [%][b)]	E_g^{onset} [eV][c)]	E_{loss} [eV][d)]
PBDT-2FBn:IT-4F	Inverted	CB 0.5 vol% DIO	0.838 (0.837 ± 0.001)	18.3 (17.45) (18.2 ± 0.20)	59.3 (58.3 ± 1.00)	9.1 (9.02)	1.50	0.66
PBDT-2FBn:IT-4F	Conventional	CB 0.5 vol% DIO	0.858 (0.857 ± 0.001)	18.0 (17.45) (17.0 ± 1.20)	60.2 (58.2 ± 2.00)	9.3 (9.02)		
PBDT-2FBn:BTP-BO-4Cl	Conventional	CB 1 vol% CN	0.878 (0.863 ± 0.015)	18.0 (17.34) (17.0 ± 1.10)	64.6 (61.05 ± 3.55)	10.2 (9.56)	1.35	0.47
PBDT-4FBn:IT-4F	Inverted	CB 0.5 vol% DIO	0.899 (0.879 ± 0.002)	17.3 (16.12) (16.2 ± 1.10)	55.1 (55.1 ± 0.22)	8.6 (8.41)	1.50	0.60
PBDT-4FBn:IT-4F	Conventional	CB 0.5 vol% DIO	0.899 (0.886 ± 0.004)	16.2 (15.97) (16.1 ± 0.15)	56.3 (54.0 ± 2.30)	8.2 (7.66)		

Device architecture: ITO/ZnO/active layer/MoO_3/Ag (Inverted); ITO/PEDOT:PSS/active layer/PDINN/Ag (conventional); [a)] The integral J_{sc} in parentheses is obtained from the EQE curves; [b)] The average values and standard deviations were derived from eight to ten independent devices; [c)] E_g^{onset} is the optical gap of the main light absorber, which is calculated from the EQE spectrum; [d)] $E_{loss} = E_g^{onset} - qV_{oc}$, where q is the elementary charge.[59]

were mainly driven by the improvement in the J_{sc} from 16.2 to 17.3 mA cm^{-2}, which could be originated from more intense absorption of the inverted devices over conventional ones, which resulted from different sequences and optical properties of each composing interlayer as indicated in previous reports.[56,57] Moreover, these observations were in good agreement with external quantum efficiency (EQE) profiles, as shown in Figure 4b,d. Overall, negligible differences in photovoltaic performances exclude the possible effects of device configuration on the performance of these polymer blends. Therefore, we further studied the impact of fluorination on overall photovoltaic parameters. As expected, enabled by the presence of multiple F-substituents in the molecular structures, both these polymers displayed high V_{oc} in the 0.838–0.899 V. Besides, the highest V_{oc} in PBDT-4FBn case is consistent with its deeper HOMO energy levels of polymers induced by the insertion of 4FBn unit. Conversely,

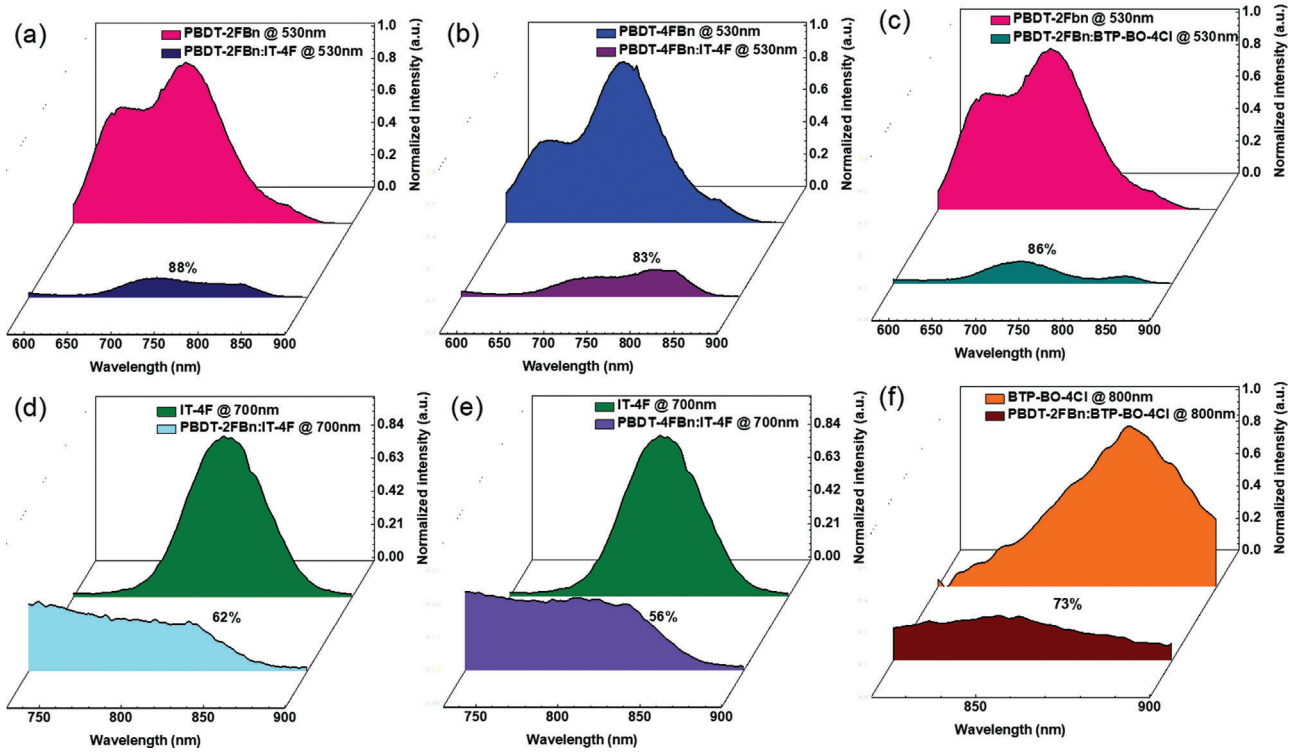

Figure 5. PL spectra of a,c) PBDT-2FBn and b) PBDT-4FBn (excited at 530 nm), d,e) IT-4F (excited at 700 nm), f) BTP-BO-4Cl (excited at 800 nm), as well as blend films of PBDT-2FBn:IT-4F and PBDT-4FBn:IT-4F (excited at 530 nm [a,b] and 700 nm [d,e]) and PBDT-2FBn:BTP-BO-4Cl (excited at 530 nm [c] and 800 nm [f]).

PBDT-4FBn:IT-4F-based devices displayed lower J_{sc} and FF than PBDT-2FBn counterparts, leading to a lower PCE. These trends further substantiate previous reports, which suggest that excessive fluorination in polymer could hamper the trade-off between J_{sc} and V_{oc}.[52,58]

Recently, "Y-class" NFAs have created hope for the practical reality of commercialization of OSCs by breaking the 15% PCE barrier and various impressive PCEs over 17% have been realized recently by employing this class of acceptor along with efficient donor polymers.[13] Hence, we further tested our best-performing polymer PBDT-2FBn by mixing with BTP-BO-4Cl acceptor with complementary absorption and good energy level alignment to further enhance the photovoltaic performance. The detailed screening of PBDT-2FBn:BTP-BO-4Cl blends by varying blend ratio, active layer thickness, and solvent additives were given in Figures S8–S10 and Tables S3–S5, Supporting Information. The champion PBDT-2FBn:BTP-BO-4Cl (1:1.1)-based devices fabricated with conventional structure and 1 vol% CN yielded the best PCE of 10.2% with remarkable V_{oc} of 0.878 V, J_{sc} of 18.0 mA cm^{-2}, and FF of 64.6%. Relative to PBDT-4FBn:IT-4F-based devices, PBDT-2FBn:BTP-BO-4Cl blend gave similar J_{sc}, but they afforded significantly elevated V_{oc} and FF. Additionally, device energy losses (E_{loss}) are estimated from the equation $E_{loss} = E_g - qV_{oc}$ (E_g^{onset} was obtained from the EQE spectrum) (Table 2).[59] Notably, the PBDT-2FBn:IT-4F, PBDT-4FBn:IT-4F, and PBDT-2FBn:BTP-BO-4Cl devices showed reduced E_{loss} of 0.66, 0.60, and 0.47 eV, respectively. Interestingly, PBDT-2FBn:BTP-BO-4Cl device displayed an unprecedented lowest of 0.47 eV, which was rarest among a few examples having E_{loss} <0.5 eV reported to date.[60–62]

To comprehensively understand the reason behind the origin of variation in J_{sc} values, the EQE profiles of the optimal devices were studied. As shown in Figures 4b,d, both PBDT-2FBn or PBDT-4FBn:IT-4F-based devices displayed broad photo-response ranging from 400 to 800 nm, ascribed from the complementary absorption of the blend components. Furthermore, relative to PBDT-4FBn-based devices, PBDT-2FBn:IT-4F blend delivered a much higher EQE response along the entire wavelength region in both conventional and inverted cases, along with maximum EQE exceeding >70% at ≈750, thereby producing higher photocurrent in OSCs and consistent with its higher absorption coefficients values. Besides, compared to PBDT-2FBn:IT-4F-based films, PBDT-2FBn:BTP-BO-4Cl blend exhibited slightly lower EQE response (EQE values over 55% along 300–900 nm except for the valley region around 600 nm), but is compensated by extended absorption range ≈900 nm induced from the BTP-BO-4Cl acceptor which helped to offset this J_{sc} loss. Also, integrated J_{sc} obtained from EQE curves were in accordance with those extracted from *J*–*V* measurements within the permissible deviation range.

The photoluminescence (PL) quenching tool was used to gather information regarding the degree of phase separation and the photoinduced charge transfer in these optimal blend films (**Figure 5**). Based on the absorption profiles of polymers and NFAs units (IT-4F and BTP-BO-4Cl), the excitation wavelength was fixed as 530, 700, and 800 nm, respectively, and

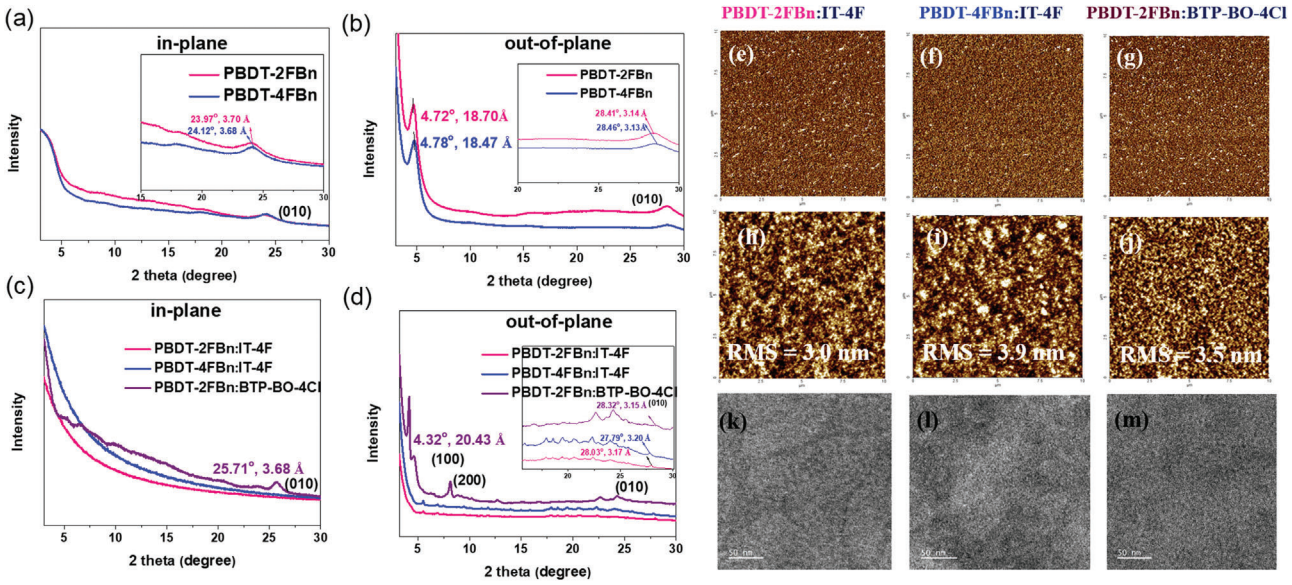

Figure 6. a,c) In-plane (q_{xy}) and b,d) out-of-plane (q_z) line cut profiles of the pristine a,b) PBDT-2FBn and PBDT-4FBn, and c,d) PBDT-2FBn:IT-4F, PBDT-4FBn:IT-4F, and PBDT-2FBn:BTP-BO-4Cl-based blends, respectively, obtained from X-ray diffraction study and tapping mode AFM e–g) phase, h–j) height, and k–m) TEM images of e,h,k) PBDT-2FBn:IT-4F, f,i,l) PBDT-4FBn:IT-4F, and g,j,m) PBDT-2FBn:BTP-BO-4Cl blend films, respectively.

corresponding PL spectra were recorded for pristine polymers, NFAs, and optimal blend films. Notably, both PBDT-2FBn:IT-4F and PBDT-2FBn:BTP-BO-4Cl blend exhibits efficient PL quenching over 85% relative to pristine PBDT-2FBn (exited at 530 nm). In comparison, the same films showed 62% and 73% quenching relative to pure IT-4F and BTP-BO-4Cl acceptor units (exited at 700 and 800 nm, respectively). Conversely, despite effective PL quenching ≈90% when excited at 530 nm, PBDT-4FBn:IT-4F films exhibit the poorest quenching of 56% (when excited at 700 nm). These results suggest that all the photoinduced exciton formed in both PBDT-2FBn:IT-4F and PBDT-2FBn:BTP-BO-4Cl blend were effectively dissociated into free charge carriers through photoinduced electron or hole transfer pathways than in the case of PBDT-4FBn:IT-4F blend film, which agrees well with higher EQE values and J_{sc} in the corresponding OSCs.[38,42,63–65]

As high and balanced charge carrier mobilities and optimal phase separated-morphology is necessary to realize the high J_{sc} and FF, so first hole and electron mobilities (μ_h and μ_e) optimal blend films were investigated by fabricating electron-only (ITO/ZnO/active-layer/PDINN/Ag) and hole-only (ITO/PEDOT:PSS/active layer/MoO_3/Ag) devices, respectively, using space-charge-limited current (SCLC) method (Figure S11, Supporting Information). The calculated μ_e and μ_h for PBDT-2FBn:IT-4F and PBDT-4FBn:IT-4F-based blend films are $6.81 \times 10^{-4}/4.39 \times 10^{-4}$ and $6.57 \times 10^{-4}/3.05 \times 10^{-4}$ cm^{-2} V^{-1} s^{-1}, respectively. Moreover, higher μ_h and μ_e of PBDT-2FBn:IT-4F further improved the μ_e/μ_h ratio from 2.15 (in PBDT-4FBn:IT-4F) to 1.55, thus justifying its higher J_{sc} and FF in the devices. After mixing of PBDT-2FBn with the BTP-BO-4Cl acceptor, μ_e and μ_h of corresponding blends were further enhanced to $7.16 \times 10^{-4}/5.86 \times 10^{-4}$ cm^{-2} V^{-1} s^{-1} with μ_e/μ_h ratio of 1.22. Thus, favorable molecular ordering and higher and balanced charge mobilities are partly responsible for improving FF, J_{sc}, and overall PCEs by promoting charge extraction and collection by suppressing charge recombination.

X-ray diffraction analysis of pristine polymers and blends was performed to investigate the effect of different F-content in polymers on the molecular ordering and crystallinities. Figure 5 depicts the in-plane (IP, q_{xy}) and out-of-plane (OOP, q_z) profiles of the XRD. As cast films of PBDT-2FBn and PBDT-4FBn showed lamellar diffraction (100) at 2θ of 4.72° and 4.78° along OOP direction, which corresponds to a lamellar spacing distance of 18.70 and 18.47 Å, respectively. Additionally, they also showed intense (010) π–π stacking peaks along both IP and OOP directions (**Figure 6**a,b). The π–π stacking distances were estimated as 3.70/3.14 Å (for PBDT-2FBn) and 3.68/3.13 Å (for PBDT-4FBn), respectively, for IP/OOP directions. These results clearly show the coexistence of "face-on" and "edge-on" orientations in both polymers. Furthermore, reduced lamellar and π–π spacing of PBDT-4FBn than PBDT-2FBn implied that PBDT-4FBn has higher crystallinity due to its coplanar backbone facilitated by noncovalent F···H and F···S Coulombic interactions. Interestingly, when blended with IT-4F, π–π stacking peaks along IP has vanished entirely (Figure 6c,d). Still, they retained along OOP directions suggesting the variation of molecular ordering from mixed to "face-on" is beneficial for vertical charge transport in OSCs.[19,42,66,67] Interestingly, the addition of IT-4F led to a lower d-spacing distance of 3.17 Å in than PBDT-2FBn:IT-4F (vs 3.20 Å for PBDT-4FBn:IT-4F), which aided more efficient and balanced charge transport in SCLC devices. Last, PBDT-2FBn:BTP-BO-4Cl has a high degree of molecular ordering among the studied blends, as revealed by the more assertive (100) and (200) diffraction peaks and pronounced π–π stacking peak with shorter d-spacing in both IP and OOP directions. Such a privileged molecular ordering justifies its excellent charge carrier mobilities and enhances photovoltaic performance.

Finally, bulk morphology and film microstructures of the blends were examined using atomic force microscopy (AFM) and transmission electron microscopy (TEM). As shown in AFM images Figure 6e,h, PBDT-2FBn:IT-4F blend displayed much homogenous and smooth morphology with a relative root-mean-square (RMS) roughness of 3.0 nm, indicating good intermixing of the blend components. Whereas PBDT-4FBn:IT-4F blends display much phase-segregated morphology with large cluster zones leading to an increased RMS roughness of 3.9 nm (Figure 6f,i). This higher roughness may be ascribed from the strong excessive intermolecular F···H and F···S interaction and self-agglomeration caused by the fluorination.[52,58,68] Moreover, few reports indicated that excessive fluorination could lead to high aggregation and lower solubility, thus greatly influencing morphology and miscibility.[69,70] Such a type of phase segregated morphology proved to cause a negative effect on exciton migration by reducing the exciton diffusion length. Additionally, they also act as charge traps that promote higher charge recombination. Thus, inferior morphology of PBDT-4FBn:IT-4F accounts for poor J_{SC}, FF, and low PCE. Meanwhile, incorporating BTP-BO-4Cl into PBDT-2FBn produced bicontinuous nanofibrillar structures with appropriate small domain sizes (≈10 nm) and RMS roughness further reduced to 3.5 nm (Figure 6g,j). These distinctive morphological features benefit exciton dissociation and charge transfer by forming charge transport pathways[42] and correlated well with PL data, higher charge carrier mobilities, and PCEs of PBDT-2FBn:BTP-BO-4Cl films. Furthermore, TEM images (Figure 6k–m) further substantiated AFM data, where both PBDT-2FBn:IT-4Fand PBDT-2FBn:BTP-BO-4Cl-based blend films showed fibril-like finely distributed structures than PBDT-4FBn:IT-4F counterparts. Such nanofibrillar crystalline morphology with a well-percolated bicontinuous network of donor and acceptor phases will aid in promoting efficient charge transport, increasing the J_{SC} and FF values in corresponding OSCs.[49,63] However, relatively large aggregates of PBDT-4FBn:IT-4F emphasize reduced miscibility between the PBDT-4FBn and IT-4F phases, which could induce unfavorable exciton recombination and hence resulted in reduced photovoltaic performances.

3. Conclusion

In conclusion, two new low-cost WBG donors, PBDT-2FBn and PBDT-4FBn based on alternate fluorinated-thienyl benzodithiophene donor and 2FBn or 4FBn, respectively, were designed and synthesized via sequential fluorination strategy. Though both polymers demonstrated similar optical properties with a large bandgap of 2.12 to 2.15 eV, respectively, the sequential fluorination gradually downshifted HOMO energy levels ranging from PBDT-2FBn to PBDT-4FBn (5.52 vs −5.63 eV) and improved coplanarity and crystallinity. When mixed with compatible IT-4F acceptor units having complementary absorption and well-matched energy levels, PBDT-2FBn:IT-4F exhibits appropriate phase separation morphology with favorable molecular orientation and good miscibility than PBDT-4FBn:IT-4F. As a result, PBDT-2FBn:IT-4F-based OSCs showed the highest PCE of 9.3% with ≈8% enhancement from the PBDT-4FBn-based devices (8.6%). Moreover, further mixing of PBDT-2FBn with BTP-BO-4Cl acceptor unit further improved absorption range and helped to realize privileged morphology with ideal domain sizes for efficient exciton dissociation and charge transport; hence PCE was significantly enhanced to 10.2% with remarkably low energy loss of 0.46 eV. Thus, our works demonstrate that the use of BDT-alt-heteroarenes-based inexpensive and scalable polymer design, along with crystallinity and energy level modulation by sequential fluorination, is a successful strategy to construct efficient WBG donors for non-fullerene OSCs.

Supporting Information

Supporting Information is available from the Wiley Online Library or from the author.

Acknowledgements

This paper was supported by Konkuk University Researcher Fund in 2020, the Korea Institute of Energy Technology Evaluation and Planning (KETEP), the Ministry of Trade, Industry & Energy (MOTIE) of the Republic of Korea (Nos. 2018201010636A), and the National Research Foundation of Korea (NRF) (No. 2020R1A2C2010916 and 2021M3H4A1A03039591).

Conflict of Interest

The authors declare no conflict of interest.

Data Availability Statement

The data that support the findings of this study are available in the Supporting Information of this article.

Keywords

fluorine effect, high open-circuit voltage, low photon energy loss, low-cost polymer donor, non-fullerene solar cells, wide-bandgap donors

Received: January 27, 2022
Revised: February 21, 2022
Published online:

[1] A. J. Heeger, *Adv. Mater.* **2014**, *26*, 10.
[2] L. Lu, T. Zheng, Q. Wu, A. M. Schneider, D. Zhao, L. Yu, *Chem. Rev.* **2015**, *115*, 12666.
[3] R. Xue, J. Zhang, Y. Li, Y. Li, *Small* **2018**, *14*, 1801793.
[4] Y. Lin, Y. Jin, S. Dong, W. Zheng, J. Yang, A. Liu, F. Liu, Y. Jiang, T. P. Russell, F. Zhang, F. Huang, L. Hou, *Adv. Energy Mater.* **2018**, *8*, 1701942.
[5] T. Yan, W. Song, J. Huang, R. Peng, L. Huang, Z. Ge, *Adv. Mater.* **2019**, *31*, 1902210.
[6] G. P. Kini, S. J. Jeon, D. K. Moon, *Adv. Funct. Mater.* **2021**, *31*, 2007931.
[7] X. Du, T. Heumueller, W. Gruber, A. Classen, T. Unruh, N. Li, C. J. Brabec, *Joule* **2019**, *3*, 215.
[8] Z. Zhang, J. Yuan, Q. Wei, Y. Zou, *Front. Chem.* **2018**, *6*, 414.
[9] S. Dey, *Small* **2019**, *15*, 1900134.
[10] G. Zhang, J. Zhao, P. C. Y. Chow, K. Jiang, J. Zhang, Z. Zhu, J. Zhang, F. Huang, H. Yan, *Chem. Rev.* **2018**, *118*, 3447.
[11] C. Li, H. Fu, T. Xia, Y. Sun, *Adv. Energy Mater.* **2019**, *9*, 1900999.

[12] H. Wang, J. Cao, J. Yu, Z. Zhang, R. Geng, L. Yang, W. Tang, *J. Mater. Chem. A* **2019**, *7*, 4313.
[13] S. Li, C.-Z. Li, M. Shi, H. Chen, *ACS Energy Lett.* **2020**, *5*, 1554.
[14] S. Li, X. Yuan, Q. Zhang, B. Li, Y. Li, J. Sun, Y. Feng, X. Zhang, Z. Wu, H. Wei, M. Wang, Y. Hu, Y. Zhang, H. Y. Woo, J. Yuan, W. Ma, *Adv. Mater.* **2021**, *33*, 2101295.
[15] Y. Cui, H. Yao, J. Zhang, T. Zhang, Y. Wang, L. Hong, K. Xian, B. Xu, S. Zhang, J. Peng, Z. Wei, F. Gao, J. Hou, *Nat. Commun.* **2019**, *10*, 2515.
[16] Y. Cui, H. Yao, L. Hong, T. Zhang, Y. Tang, B. Lin, K. Xian, B. Gao, C. An, P. Bi, W. Ma, J. Hou, *Natl. Sci. Rev.* **2019**, *7*, 1239.
[17] Q. Liu, Y. Jiang, K. Jin, J. Qin, J. Xu, W. Li, J. Xiong, J. Liu, Z. Xiao, K. Sun, S. Yang, X. Zhang, L. Ding, *Sci. Bull.* **2020**, *65*, 272.
[18] L. Zhan, S. Li, T.-K. Lau, Y. Cui, X. Lu, M. Shi, C.-Z. Li, H. Li, J. Hou, H. Chen, *Energy Environ. Sci.* **2020**, *13*, 635.
[19] S. Li, L. Ye, W. Zhao, H. Yan, B. Yang, D. Liu, W. Li, H. Ade, J. Hou, *J. Am. Chem. Soc.* **2018**, *140*, 7159.
[20] J. Chen, G. Li, Q. Zhu, X. Guo, Q. Fan, W. Ma, M. Zhang, *J. Mater. Chem. A* **2019**, *7*, 3745.
[21] J. Wu, Q. Fan, M. Xiong, Q. Wang, K. Chen, H. Liu, M. Gao, L. Ye, X. Guo, J. Fang, Q. Guo, W. Su, Z. Ma, Z. Tang, E. Wang, H. Ade, M. Zhang, *Nano Energy* **2021**, *82*, 105679.
[22] A. Tang, W. Song, B. Xiao, J. Guo, J. Min, Z. Ge, J. Zhang, Z. Wei, E. Zhou, *Chem. Mater* **2019**, *31*, 3941.
[23] X. Wang, A. Tang, J. Yang, M. Du, J. Li, G. Li, Q. Guo, E. Zhou, *Sci. China: Chem.* **2020**, *63*, 1666.
[24] F. Zhao, J. Zhou, D. He, C. Wang, Y. Lin, *J. Mater. Chem. C* **2021**, *9*, 15395.
[25] X. Yuan, Y. Zhao, T. Zhan, J. Oh, J. Zhou, J. Li, X. Wang, Z. Wang, S. Pang, P. Cai, C. Yang, Z. He, Z. Xie, C. Duan, F. Huang, Y. Cao, *Energy Environ. Sci.* **2021**, *14*, 5530.
[26] G. P. Kini, H. S. Park, S. J. Jeon, Y. W. Han, D. K. Moon, *Sol. Energy* **2020**, *207*, 720.
[27] Q. Fan, W. Su, X. Meng, X. Guo, G. Li, W. Ma, M. Zhang, Y. Li, *Sol. RRL* **2017**, *1*, 1700020.
[28] M. Zhang, X. Guo, S. Zhang, J. Hou, *Adv. Mater.* **2014**, *26*, 1118.
[29] Y. Zhang, H. Yao, S. Zhang, Y. Qin, J. Zhang, L. Yang, W. Li, Z. Wei, F. Gao, J. Hou, *Sci. China: Chem.* **2018**, *61*, 1328.
[30] Q. Guo, Q. Guo, Y. Geng, A. Tang, M. Zhang, M. Du, X. Sun, E. Zhou, *Mater. Chem. Front.* **2021**, *5*, 3257.
[31] Z. Wang, X. Xu, Z. Li, K. Feng, K. Li, Y. Li, Q. Peng, *Adv. Electron. Mater.* **2016**, *2*, 1600061.
[32] K. Wang, W. Su, X. Guo, M. Zhang, Y. Li, *Org. Electron.* **2016**, *33*, 15.
[33] G. P. Kini, J. Y. Choi, S. J. Jeon, I. S. Suh, D. K. Moon, *Dyes Pigm.* **2019**, *164*, 62.
[34] C. Cui, Z. He, Y. Wu, X. Cheng, H. Wu, Y. Li, Y. Cao, W.-Y. Wong, *Energy Environ. Sci.* **2016**, *9*, 885.
[35] R. K. Pai, T. N. Ahipa, B. Hemavathi, *RSC Adv.* **2016**, *6*, 23760.
[36] L. Ye, S. Zhang, L. Huo, M. Zhang, J. Hou, *Acc. Chem. Res.* **2014**, *47*, 1595.
[37] G. P. Kini, S. R. Suranagi, M. Kumar, R. Singh, *Dyes Pigm.* **2020**, *175*, 108083.
[38] W. Su, G. Li, Q. Fan, Q. Zhu, X. Guo, J. Chen, J. Wu, W. Ma, M. Zhang, Y. Li, *J. Mater. Chem. A* **2019**, *7*, 2351.
[39] M. Du, Y. Geng, H. Ji, G. Li, Y. Xiao, K. Zuo, Y. Liu, Q. Guo, A. Tang, E. Zhou, *Dyes Pigm.* **2021**, *194*, 109609.
[40] J. Zhao, Y. Li, G. Yang, K. Jiang, H. Lin, H. Ade, W. Ma, H. Yan, *Nat. Energy* **2016**, *1*, 15027.
[41] Q. Zhang, M. A. Kelly, N. Bauer, W. You, *Acc. Chem. Res.* **2017**, *50*, 2401.
[42] J. Yang, M. A. Uddin, Y. Tang, Y. Wang, Y. Wang, H. Su, R. Gao, Z.-K. Chen, J. Dai, H. Y. Woo, X. Guo, *ACS Appl. Mater. Interfaces* **2018**, *10*, 23235.
[43] Q. Fan, U. A. Méndez-Romero, X. Guo, E. Wang, M. Zhang, Y. Li, *Chem. - Asian J.* **2019**, *14*, 3085.
[44] G. P. Kini, J. Y. Choi, S. J. Jeon, I. S. Suh, D. K. Moon, *Polymer* **2018**, *148*, 330.
[45] J. Yuan, Y. Zhang, L. Zhou, G. Zhang, H.-L. Yip, T.-K. Lau, X. Lu, C. Zhu, H. Peng, P. A. Johnson, M. Leclerc, Y. Cao, J. Ulanski, Y. Li, Y. Zou, *Joule* **2019**, *3*, 1140.
[46] T. Wang, J. Qin, Z. Xiao, J. Zhang, Z. Chen, L. Zhang, M. Cheng, Z. Jin, Y. Yuan, W.-Q. Wu, C. Duan, S. Xie, K. Sun, F. Hao, L. Ding, *Nano Energy* **2020**, *77*, 105161.
[47] J. E. Yu, S. J. Jeon, J. Y. Choi, Y. W. Han, E. J. Ko, D. K. Moon, *Small* **2019**, *15*, 1805321.
[48] J. Yuan, M. J. Ford, Y. Zhang, H. Dong, Z. Li, Y. Li, T.-Q. Nguyen, G. C. Bazan, W. Ma, *Chem. Mater* **2017**, *29*, 1758.
[49] S.-J. Ko, Q. V. Hoang, C. E. Song, M. A. Uddin, E. Lim, S. Y. Park, B. H. Lee, S. Song, S.-J. Moon, S. Hwang, P.-O. Morin, M. Leclerc, G. M. Su, M. L. Chabinyc, H. Y. Woo, W. S. Shin, J. Y. Kim, *Energy Environ. Sci.* **2017**, *10*, 1443.
[50] Y.-J. You, C. E. Song, Q. V. Hoang, Y. Kang, J. S. Goo, D.-H. Ko, J.-J. Lee, W. S. Shin, J. W. Shim, *Adv. Funct. Mater.* **2019**, *29*, 1901171.
[51] G. P. Kini, E. J. Lee, S. J. Jeon, D. K. Moon, *Macromol. Rapid Commun.* **2021**, *42*, 2000743.
[52] X. Zhang, J. Wu, D. Wei, Y. Cai, X. Sun, *Dyes Pigm.* **2021**, *187*, 109109.
[53] D. Liu, Y. Zhang, L. Zhan, T.-K. Lau, H. Yin, P. W. K. Fong, S. K. So, S. Zhang, X. Lu, J. Hou, H. Chen, W.-Y. Wong, G. Li, *J. Mater. Chem. A* **2019**, *7*, 14153.
[54] S.-Z. Geng, W.-T. Yang, J. Gao, S.-X. Li, M.-M. Shi, T.-K. Lau, X.-H. Lu, C.-Z. Li, H.-Z. Chen, *Chin. J. Polym. Sci.* **2019**, *37*, 1005.
[55] S. Li, L. Zhan, W. Zhao, S. Zhang, B. Ali, Z. Fu, T.-K. Lau, X. Lu, M. Shi, C.-Z. Li, J. Hou, H. Chen, *J. Mater. Chem. A* **2018**, *6*, 12132.
[56] M. Li, J. Li, D. Di Carlo Rasi, F. J. M. Colberts, J. Wang, G. H. L. Heintges, B. Lin, W. Li, W. Ma, M. M. Wienk, R. A. J. Janssen, *Adv. Energy Mater.* **2018**, *8*, 1800550.
[57] Y. Zang, C.-Z. Li, C.-C. Chueh, S. T. Williams, W. Jiang, Z.-H. Wang, J.-S. Yu, A. K.-Y. Jen, *Adv. Mater.* **2014**, *26*, 5708.
[58] P. Liu, K. Zhang, F. Liu, Y. Jin, S. Liu, T. P. Russell, H.-L. Yip, F. Huang, Y. Cao, *Chem. Mater* **2014**, *26*, 3009.
[59] Y. Tang, H. Sun, Z. Wu, Y. Zhang, G. Zhang, M. Su, X. Zhou, X. Wu, W. Sun, X. Zhang, B. Liu, W. Chen, Q. Liao, H. Y. Woo, X. Guo, *Adv. Sci.* **2019**, *6*, 1901773.
[60] H. Zhang, S. Li, B. Xu, H. Yao, B. Yang, J. Hou, *J. Mater. Chem. A* **2016**, *4*, 18043.
[61] Y. Ji, L. Xu, X. Hao, K. Gao, *Sol. RRL* **2020**, *4*, 2000130.
[62] S.-S. Wan, X. Xu, J.-L. Wang, G.-Z. Yuan, Z. Jiang, G.-Y. Ge, H.-R. Bai, Z. Li, Q. Peng, *J. Mater. Chem. A* **2019**, *7*, 11802.
[63] G. P. Kini, J. Y. Choi, S. J. Jeon, I. S. Suh, D. K. Moon, *Polym. Chem.* **2019**, *10*, 4459.
[64] H. Bin, Z.-G. Zhang, L. Gao, S. Chen, L. Zhong, L. Xue, C. Yang, Y. Li, *J. Am. Chem. Soc.* **2016**, *138*, 4657.
[65] S. H. Park, G. E. Park, S. Choi, Y. U. Kim, S. Y. Park, C. G. Park, M. J. Cho, D. H. Choi, *J. Mater. Chem. C* **2018**, *6*, 7549.
[66] G. P. Kini, S. K. Lee, W. S. Shin, S.-J. Moon, C. E. Song, J.-C. Lee, *J. Mater. Chem. A* **2016**, *4*, 18585.
[67] Y. Wu, H. Yang, Y. Zou, Y. Dong, J. Yuan, C. Cui, Y. Li, *Energy Environ. Sci.* **2019**, *12*, 675.
[68] J.-L. Wang, K.-K. Liu, J. Yan, Z. Wu, F. Liu, F. Xiao, Z.-F. Chang, H.-B. Wu, Y. Cao, T. P. Russell, *J. Am. Chem. Soc.* **2016**, *138*, 7687.
[69] Q. Wang, M. Li, X. Zhang, Y. Qin, J. Wang, J. Zhang, J. Hou, R. A. J. Janssen, Y. Geng, *Macromolecules* **2019**, *52*, 4464.
[70] K. Kawashima, T. Fukuhara, Y. Suda, Y. Suzuki, T. Koganezawa, H. Yoshida, H. Ohkita, I. Osaka, K. Takimiya, *J. Am. Chem. Soc.* **2016**, *138*, 10265.
[71] W. Zhao, S. Li, H. Yao, S. Zhang, Y. Zhang, B. Yang, J. Hou, *J. Am. Chem. Soc.* **2017**, *139*, 7148.
[72] B. Lu, J. Wang, Z. Zhang, J. Wang, X. Yuan, Y. Ding, Y. Wang, Y. Yao, *Nano Select* **2021**, *2*, 2029.